Supporting Information

On-Chip Transferrable Microdisk Lasers

Sun-Wook Park[†], Min-Woo Kim[†], Kyong-Tae Park[†], Ja-Hyeon Ku[†], and You-Shin No[,†]*

This file includes:

Methods

Supporting Information Figures S1–S11

Methods

Fabrication of microdisks. The wafer structure used for the microdisk cavities includes a 100 nm thick InP (capping layer), 260 nm thick InGaAsP slab including six multi-quantum wells (MQWs), 800 nm thick InP (sacrificial layer), 100 nm thick InGaAs (etch stop layer), and GaAs substrate. After brief wet etching of the InP capping layer using diluted hydrochloric acid solution (HCl:DI = 3:1) for 6 min, electron-beam lithography (EBL) using a polymer resist (MicroChem, PMMA C4) with a thickness of ~400 nm was carried out to generate arrays of microdisk patterns. The sample was thermally treated before it was subjected to the chemically assisted ion-beam etching (CAIBE) process. The residual resist was removed by O_2-plasma for 20 min, following which wet etching in diluted hydrochloric acid solution was performed to partially remove the InP sacrificial layer and form a submicron-sized InP-post.

Fabrication of Si-posts. A silicon-on-insulator (SOI) wafer with 260 nm thick Si, 3 µm thick SiO_2, and a Si substrate was used to fabricate the Si-posts. Another round of EBL using the same PMMA resist was performed to define the post patterns on the wafer. Reactive ion etching (RIE) was used to produce an array of microscale Si-posts. The residual resist was removed by O_2-plasma for 20 min. Before micro-transfer printing, another round of O_2-plasma treatment was carried out with the Si-posts to create a reactive oxidation layer that helps to increase the interface interaction between the microdisks and Si-posts.

Fabrication of Si master-mold. Photolithography was carried out on the 4-inch Si wafer using a photoresist (Dongjin Semichem, DNR-L300-40) to obtain an array of microcubes. Deep reactive ion etching (DRIE) was then performed to generate a microcube array with a single cubic size of 20 µm × 20 µm × 20 µm. After O_2-plasma cleaning, the Si wafer was Teflon-coated to complete the fabrication of the master-mold for microtips.

PDMS modification. The surface of the fabricated PDMS microtip was properly oxidized using either the ultraviolet (UV) illumination setup (Quark Technology, QEV-150-172) or the oxygen plasma equipment. For UV treatment, the radiation power and time were set to 10 mW and 60 s. For oxygen plasma treatment, the power and time were set to 50 W and 5 min.

Optical measurements. A function generator (RIGOL, DG4162) was connected to a temperature-controlled pulsed laser diode with a wavelength of 976 nm (Thorlab) to generate optical pulses

with a pulse width of 100 ns and duty cycle of 10%. A 50× microscope objective lens with a numerical aperture of 0.42 was used to focus the pump beam on the sample attached to the XYZ translation stage with a nanoscale translation step (Newport, M-562-XYZ). A tungsten halogen lamp (Thorlabs, OSL2) was used as the illumination source. The emitted light was sent to either an infrared (IR) camera (Hamamatsu, C12741-03) for imaging or to a monochromator (Spectral product DK480) with 1200 g/mm grating. A femtowatt InGaAs photodetector (Thorlabs, PDF10C/M) was used to detect the optical signals.

Numerical simulations. We used the finite-difference time-domain (Lumerical, FDTD Solutions) method to calculate the field profiles, quality-factors (Q-factors), and wavelengths of the resonant whispering gallery modes (WGMs) excited in the microdisk cavities. The microdisk with a diameter and thickness of 4.5 µm and 260 nm, respectively, was placed on Si-posts with various sizes, that is, 2.0–4.0 µm, and a fixed thickness of 260 nm. The refractive index of InGaAsP, Si, and SiO_2 was set to 3.4, 3.5, and 1.4, respectively. The perfectly matched layers were applied at the boundary of the calculation domain with a size of 7.0 µm × 7.0 µm × 3.0 µm and a spatial resolution of 20 nm. Dipole sources were introduced in the middle of the boundary of the microdisk to excite the resonant WGMs. For heat transfer simulation, we used the finite-element method (COMSOL-Multiphysics) to calculate both the stationary state temperature profiles and the average temperatures of the microdisk on various Si-posts and planar substrates. The Si-posts with sizes of 1.8–4.2 µm and the SiO_2/Si planar substrates with SiO_2 thicknesses of 0.2–1.0 µm were used. For the InGaAsP microdisk, thermal conductivity of 8.50 W/m·K, heat capacity of 328.45 J/kg·K and density of 5154.6 kg/m^3 at room temperature were used. The infinite element domain was used at the boundaries of the substrate in which the initial temperature was set to room temperature. The thermal insulation condition was used at the interface between the object and air. To simulate the pump-induced heat generation, the uniform volume heat source was applied to the entire volume of the microdisk. The heat density of 0.1 mW/µm^3 was determined by considering the pump laser power, spot size and volume of microdisk as well as the reflection at the surface.

Supporting Information Figures

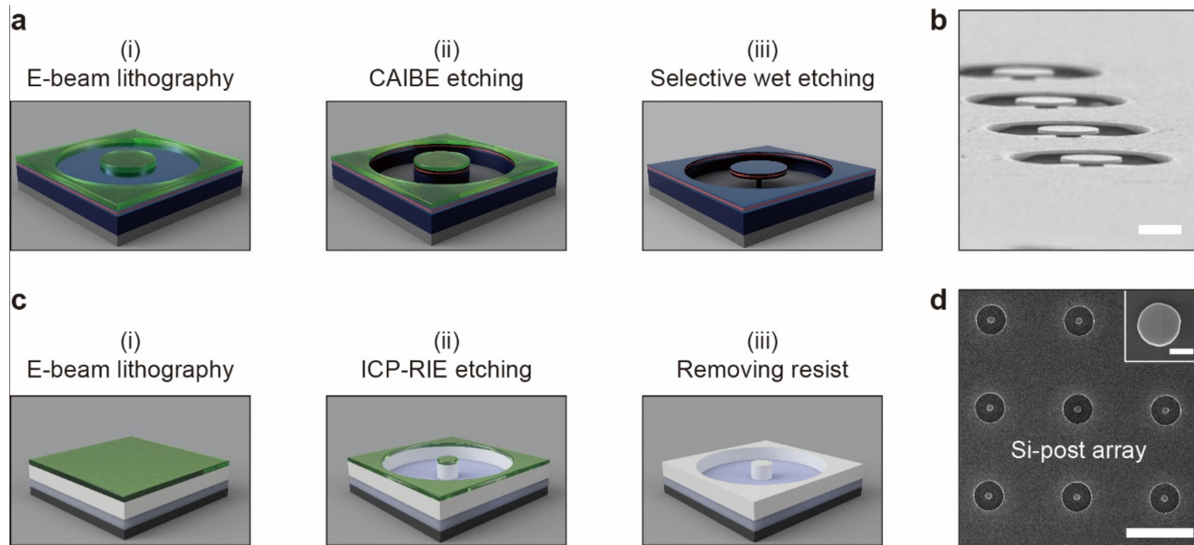

Figure S1. Fabrication of microdisk and Si-post. (a) Schematics of the key fabrication steps of microdisks. (i) Resist was spin-coated on an InGaAsP wafer, followed by EBL, to generate microdisk array patterns. (ii) Dry etching (CAIBE) was carried out to form arrays of circular cylinders. Subsequently, the O_2-plasma process removed the residual resist on the surface. (iii) The sample was dipped in diluted hydrogen chloride for ~6 min, which enabled the formation of a central InP-post with submicron size by selective and anisotropic etching of the top- and bottom-InP layers. (b) Tilted view SEM image of the fabricated InGaAsP microdisk array. Scale bar: 3 µm. (c) Schematics of the key fabrication steps of Si-posts. (i) Resist was spin-coated on an SOI wafer. Arrays of various disk patterns with different diameters were realized via EBL. (ii) ICP-RIE was carried out to form arrays of microscale Si-posts on a SiO_2 substrate. (iii) Subsequently, O_2-plasma process removed the residual resist on the surface. (d) Top-view SEM image of the fabricated Si-post array. Scale bar: 20 µm. Inset: diameter of a single post was ~1.8 µm. Scale bar: 1 µm.

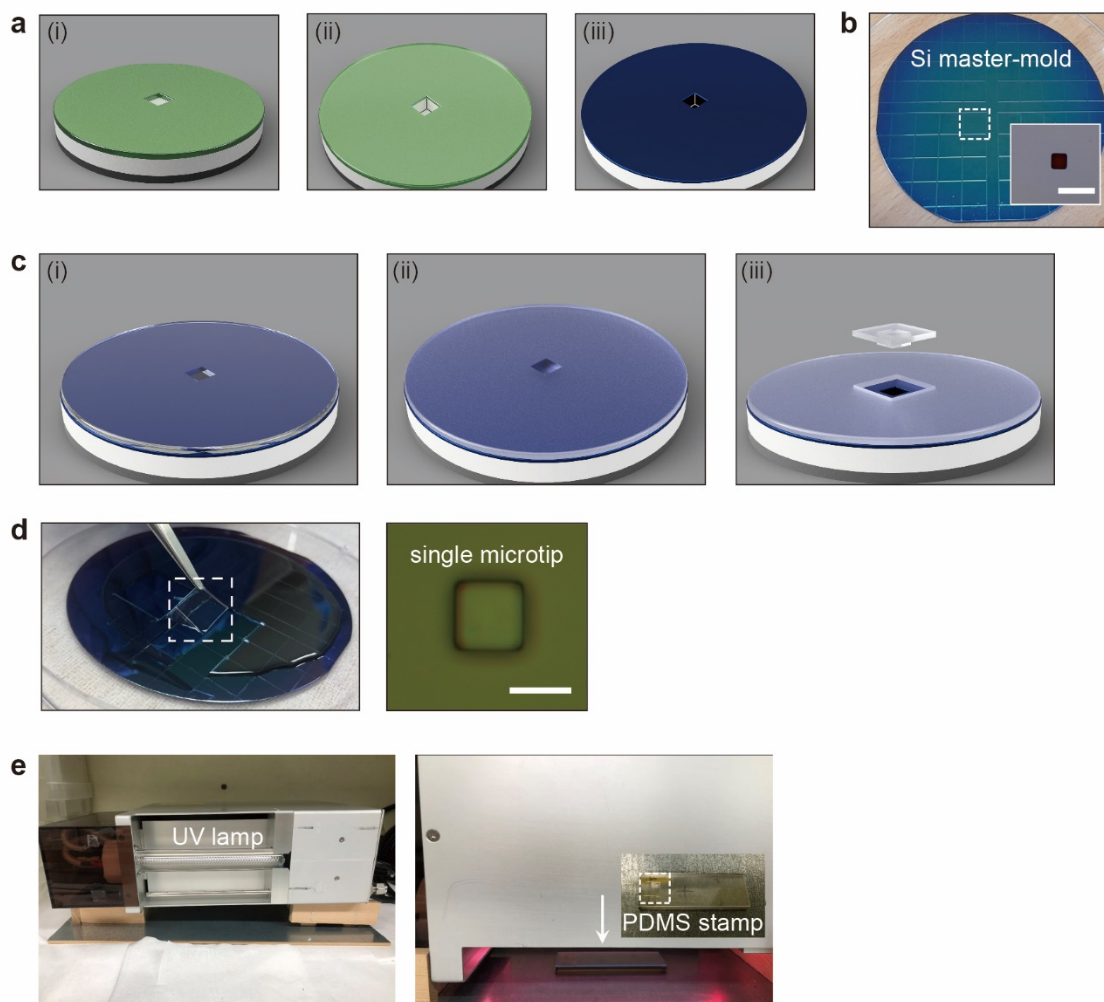

Figure S2. Fabrication of PDMS microtip. (a) Schematics of the fabrication steps of the Si master-mold: (i) Photolithography, (ii) Dry etching, and (iii) Teflon-coating. (b) Picture of the fabricated Si master-mold. Inset: optical microscope image of a single microcube. Scale bar is XX µm. (c) Schematics of the fabrication steps for PDMS microtips: (i) pouring PDMS solution (silicone elastomer base: curing agent = 10:1) on the Si master-mold, (ii) baking the wafer on a hot plate at 60 °C for 50 min, (iii) cutting a piece including a single microtip. (d) Image showing the fabricated PDMS microtip (left) and microscope image of a single microtip (right). Scale bar: 20 µm. (e) UV illumination setup for the surface modification of PDMS stamp. A stamp including the microtip is put on a slide glass for UV radiation.

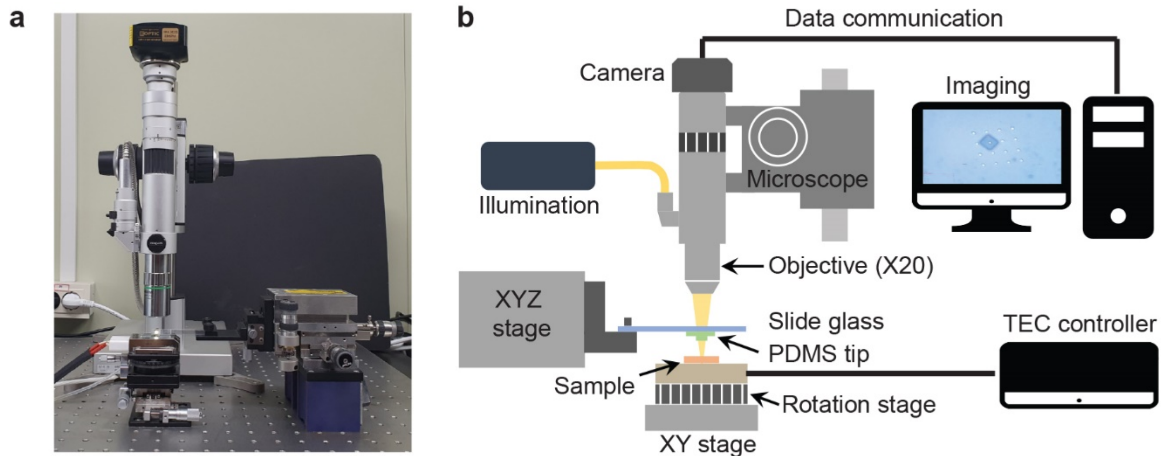

Figure S3. Micro-transfer printing setup. (a) A photograph showing the micro-transfer printing setup. (b) Schematic of the setup exhibiting the components. The PDMS stamp including a micro-tip is separated from the Si master-mold and attached to a slide glass. The slide glass is then fixed with a mount that is connected to the high-precision XYZ linear stage with minimum translation step of 100 nm (Newport, M-562-XYZ, DS-4F). The sample is mounted on a flat metal plate whose temperature is controlled thermoelectrically (MS Tech, MST-1000H). The metal plate is fixed on top of the rotational and/or linear stages. An optical microscope system (Hirox, RH-2000) including a CMOS camera (Sony, HK6.3E3s), a 20□ long working distance objective lens (Mitutoyo, M plan Apo 20×) and a white light illumination source (Fiber Optic Korea, SOL-3.0) is used to image both the PDMS stamp and the sample. The linear and angular positions of the PDMS stamp and the sample were manipulated by manually controlling the stages.

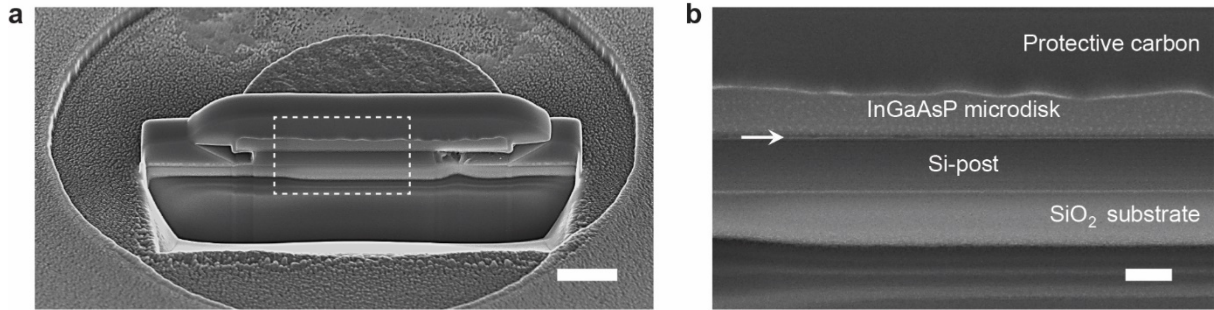

Figure S4. Cross-sectional SEM images of a transferred microdisk on a Si-post. (a) SEM image of the side view of the transferred microdisk, which was covered with a protective carbon layer and sliced by focused ion-beam (FIB) etching. The scale bar is 1 µm. (b) Magnified SEM image showing the cross-section of the white dotted box in (a). The smooth interface between the InGaAsP microdisk and Si-post reveals the high quality of bonding. A thin oxidation layer on top of Si-post (white arrow) was clearly observed. During the FIB process, the re-deposition of etching materials on the cross-sectional surface and the damage to the top surface of InGaAsP microdisk occurred. Scale bar is 200 nm.

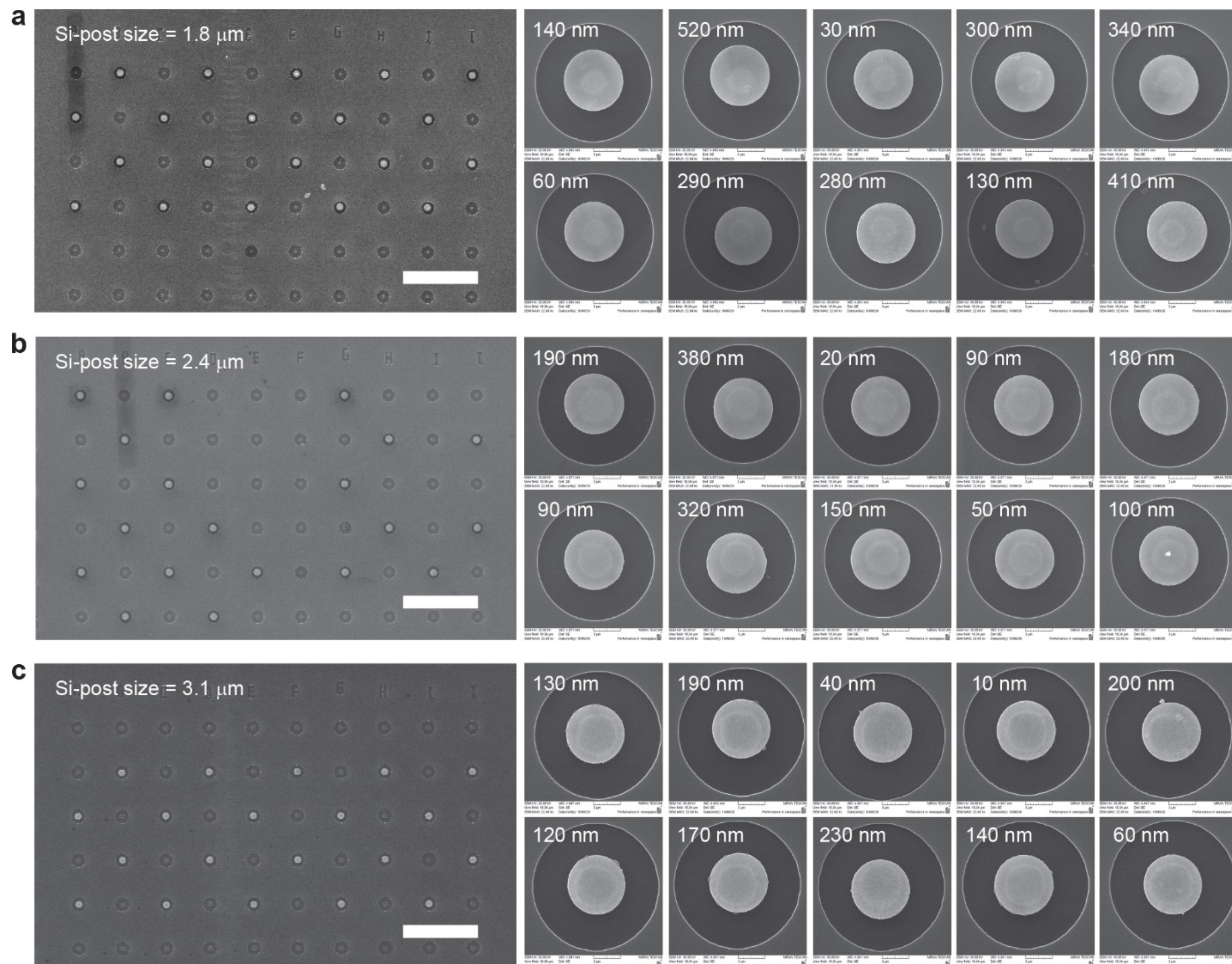

Figure S5. Misalignment measurement of the transferred microdisks on the Si-posts with different sizes. (a)–(c) Low- (left) and high-magnification (right) SEM images of the transferred microdisks on the Si-posts with size of 1.8 μm (a), 2.4 μm (b) and 3.1 μm (c), respectively. For each Si-post size, ten representative SEM images (right) were chosen to show the misalignments.

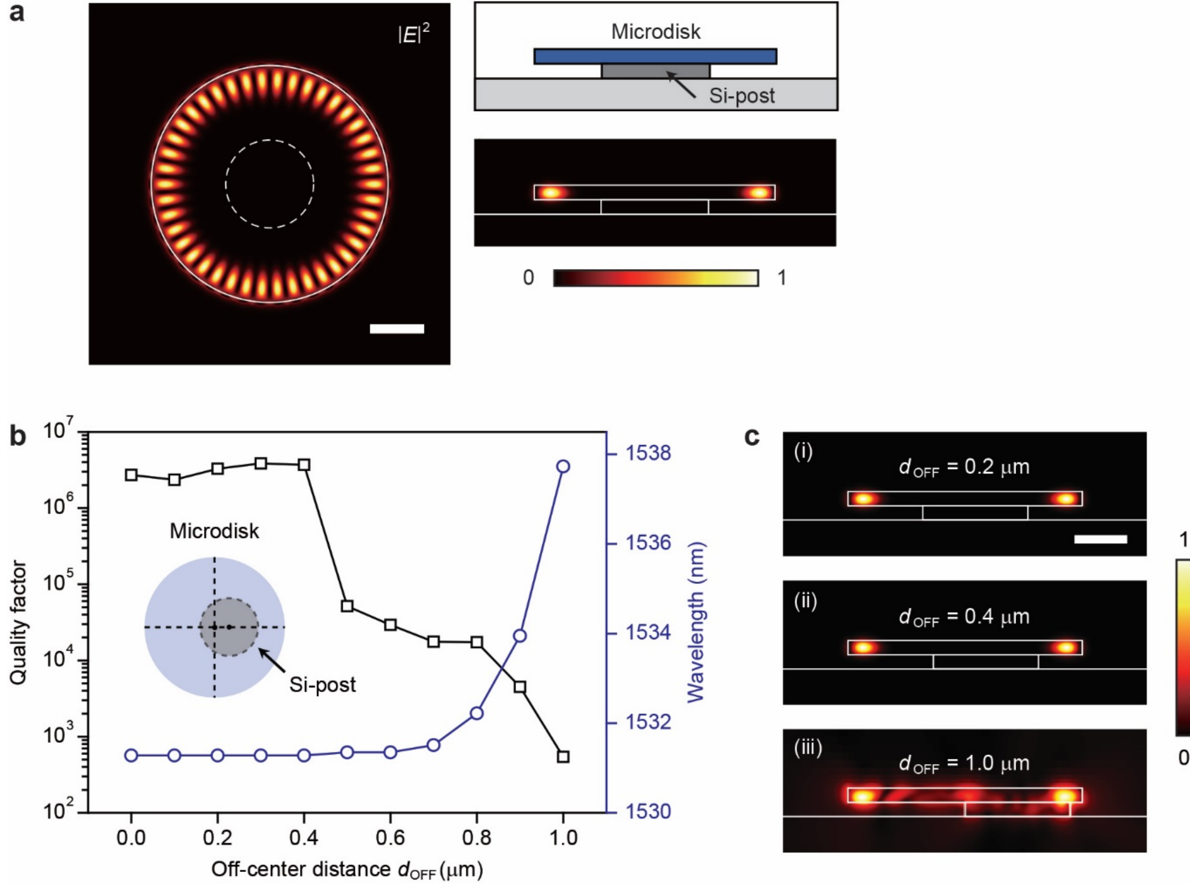

Figure S6. Numerical simulations of a transferred microdisk cavity on a Si-post. (a) Calculated electric filed intensity profiles of the WGM (azimuthal number: 21) in the transferrable microdisk cavity on a circular Si-post. Diameters of the microdisk and Si-post were set to 4.5 and 2.0 μm, respectively. The calculated *Q*-factor and resonant wavelength were ~2.5×10^6 and 1531.3 nm, respectively. The electric field intensities (side view (right) and top view (left)) were normalized by their maximum values. Scale bars are 1 μm. (b) Calculated *Q*-factors and resonant wavelengths as a function of off-center distance (d_{OFF}). Inset: schematic of the misaligned microdisk cavity and Si-post. The *Q*-factor of the cavity was considerably decreased at $d_{OFF} > 0.4$ μm and further dropped at $d_{OFF} > 0.8$ μm. The significant red-shift in resonant wavelength was observed at $d_{OFF} >$ 0.8 μm. (c) Calculated electric field intensity distributions at d_{OFF} of 0.2 μm (i), 0.4 μm (ii), and 1.0 μm (iii), respectively. Scale bar is 1 μm. The intensity distribution exhibits no noticeable perturbation or change until d_{OFF} of 0.4 μm whereas the distribution of d_{OFF} of 1.0 μm shows the significant transmission of fields toward the center of microdisk and the Si-post.

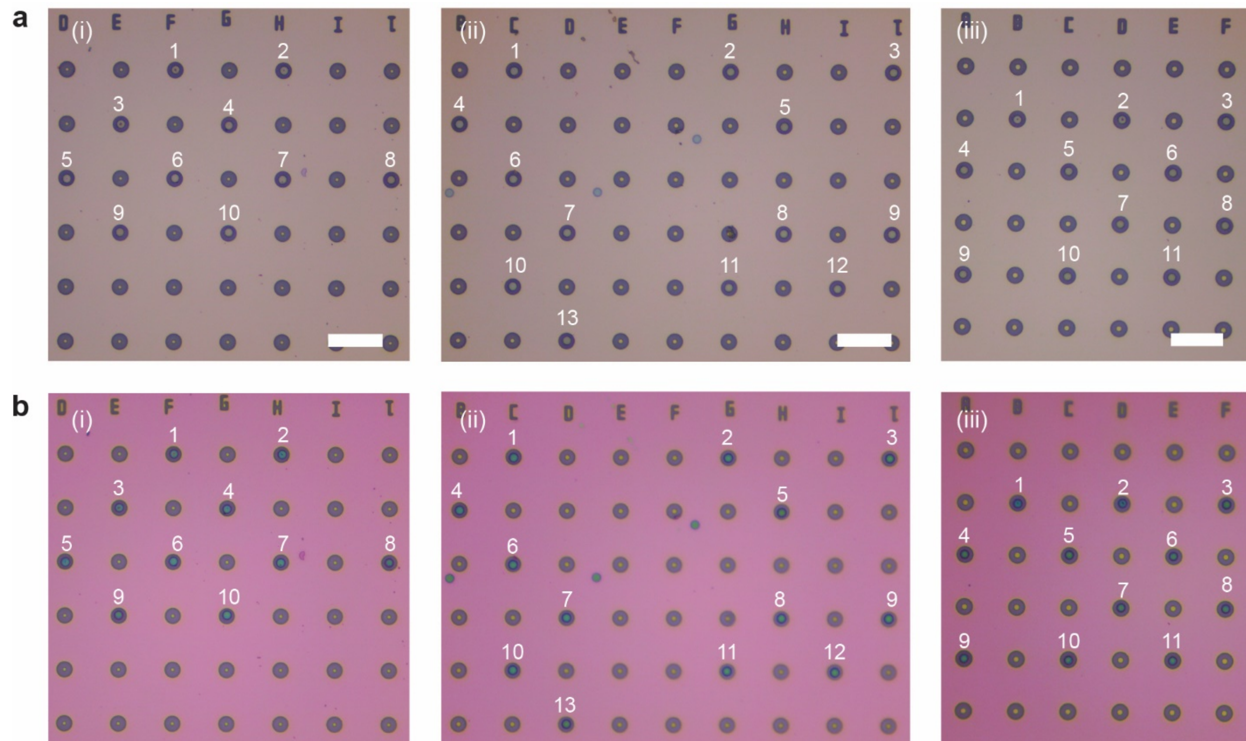

Figure S7. Mechanical stability of the transferrable microdisk devices on various Si-posts. (a) (i)–(iii) Optical microscope images of the transfer printed microdisks on Si-posts with various post sizes: 10 microdisks for d_{post} of 1.8 μm (i), 13 microdisks for d_{post} of 2.4 μm (ii) and 11 microdisks for d_{post} of 3.1 μm (iii). All the scale bars are 20 μm. (b) Optical microscope images after spin-coating with a commonly used electron beam resist (PMMA C4) at 4000 revolutions per minute. No missing microdisk was observed after the process. The result directly exhibits the mechanical stability of our device and also reveals that additional fabrications that require the electron-beam or photolithography can be processed.

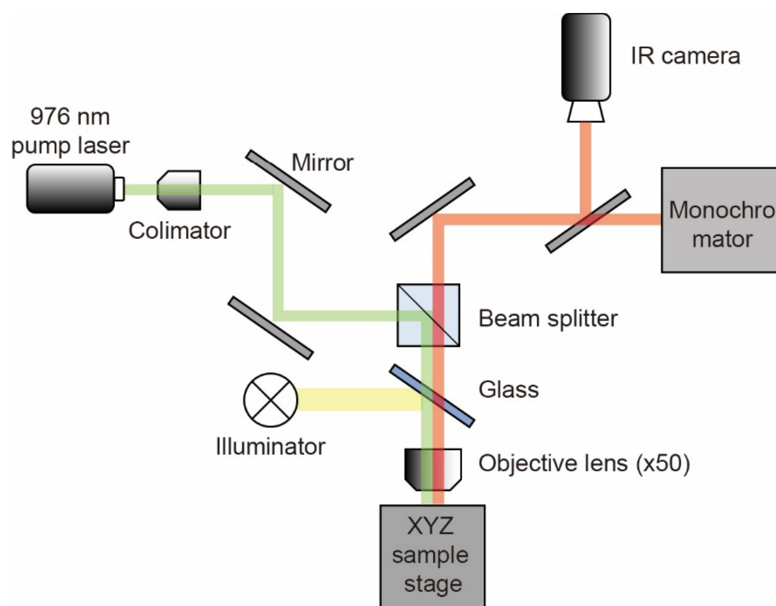

Figure S8. Schematics of optical measurement setup. A 976 nm pulsed diode laser (100-ns pulses with 10% duty cycle) was used to optically pump the transferrable microdisk lasers at room temperature. A 50× microscope objective lens with a numerical aperture of 0.42 was used to focus the pumping beam on the laser device that was attached to an XYZ micro-translation stage and to collect the light emitted by the device. The collected light was then sent to either an IR camera for imaging or a monochromator for spectroscopic analysis.

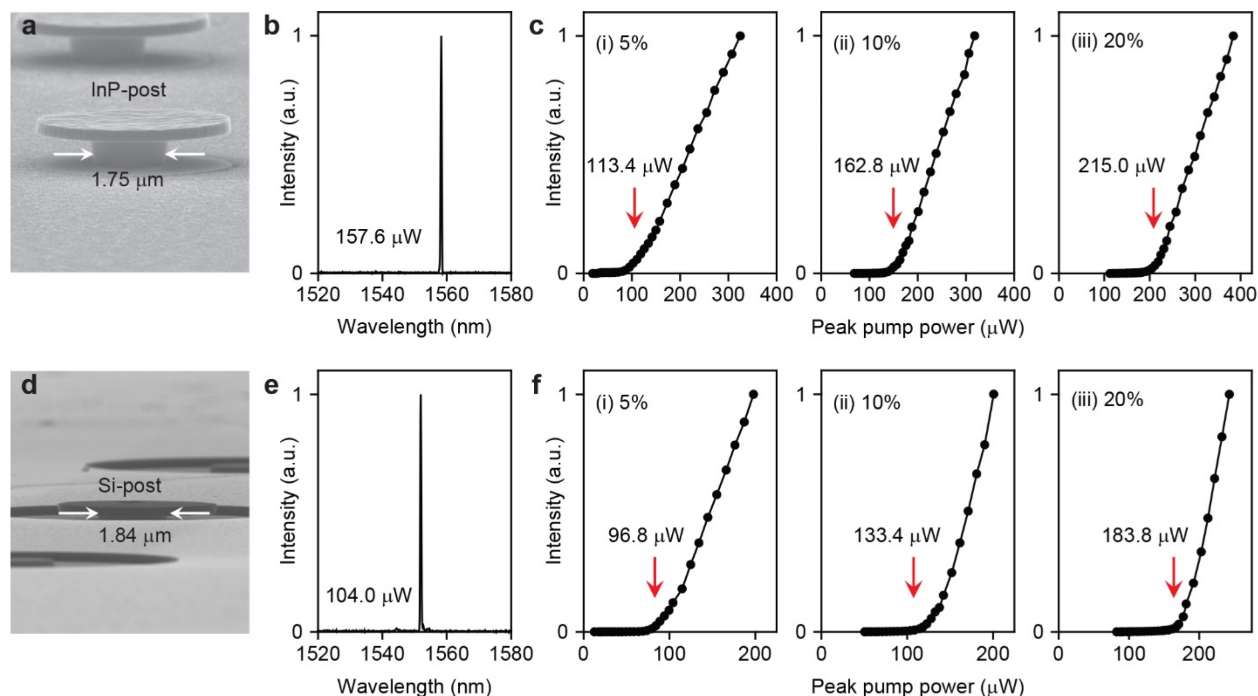

Figure S9. Pump-induced thermal effect on the microdisk lasers on the InP-post and Si-post. (a) Tilted SEM image of a microdisk supported by a chemically etched epitaxial InP-post with a hetero-interface. The diameters of microdisk and InP-post were 4.2 μm and 1.75 μm, respectively. (b) Measured spectrum showing lasing mode at 1558.3 nm obtained from the device in (a). The incident peak pump power of 157.6 μW and 5% duty ratio were used. (c) (i)–(iii) Characteristic curves obtained from the device in (a) under three different duty ratios of 5% (i), 10% (ii), and 20% (iii). The estimated thresholds were 113.4 μW, 162.8 μW and 215.0 μW for 5%, 10% and 20% duty ratios, respectively. (d) Tilted SEM image of the transferred microdisk of (a) on a Si-post with bonded interface. The diameter of Si-post was 1.84 μm. (e) Measured spectrum showing lasing mode at 1551.9 nm obtained from the device in (d). The incident pump power of 104.0 μW and the same duty ratio in (b) were used. (f) (i)–(iii) Characteristic curves obtained from the device in (d) under three different duty ratios of 5% (i), 10% (ii), and 20% (iii). The estimated thresholds were 96.8 μW, 133.4 μW and 183.8 μW for 5%, 10% and 20% duty ratios, respectively. The significantly reduced lasing thresholds were observed from the device on the Si-post for all duty ratios. In addition, the threshold difference under the same pumping condition increased as the duty ratio increased. For both lasers, the lasing thresholds were increased as the duty ratio increased.

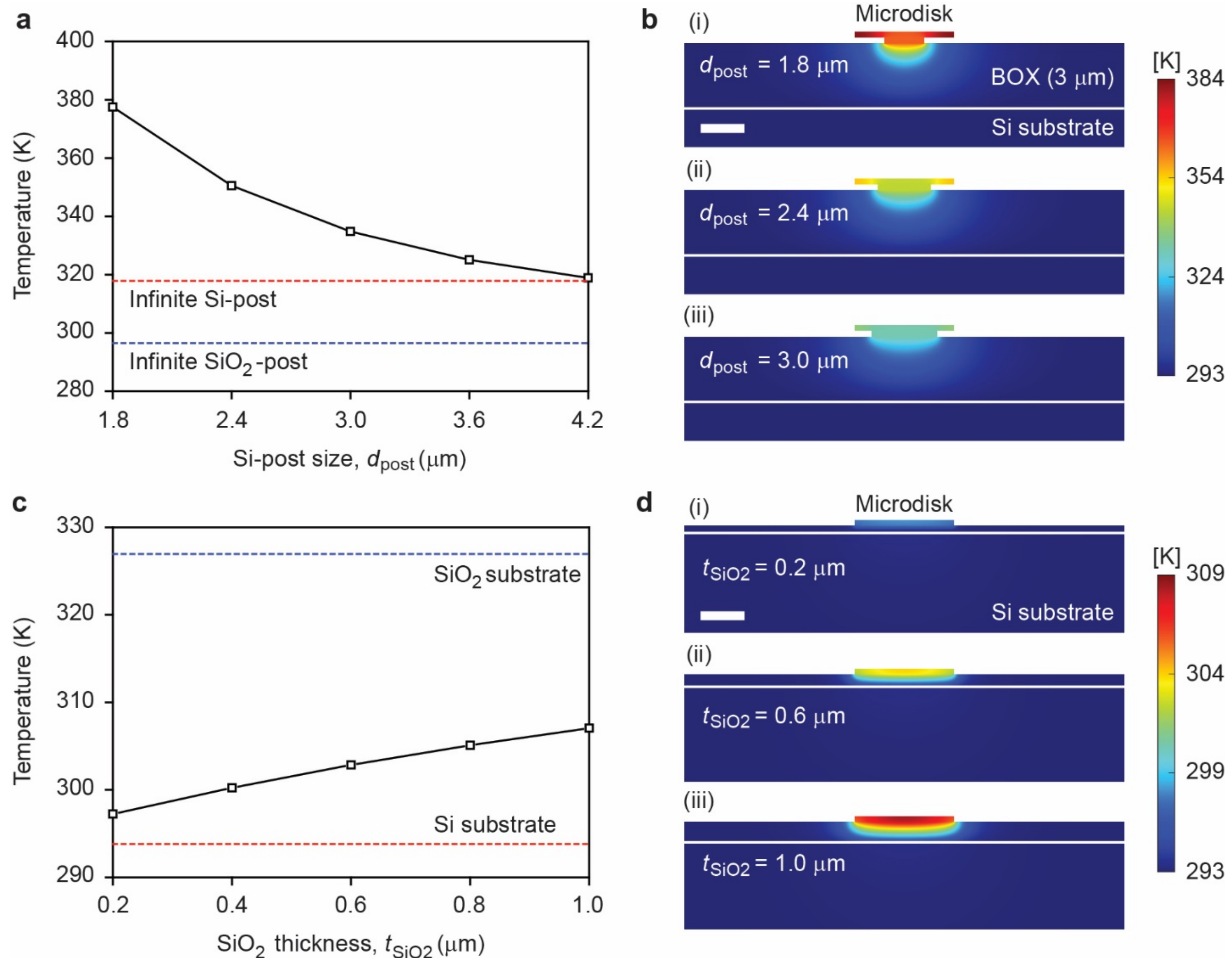

Figure S10. Numerical simulations of stationary temperature distribution in the microdisk on various Si-posts and planar substrates. (a) The calculated average temperature of the microdisk as a function of the size of Si-posts. Diameter of the microdisk was 4.5 μm and thickness of the microdisk and the Si-post was 260 nm. Thickness of the buffered oxide layer was set to 3 μm. The red and blue dotted lines indicated the microdisk on the infinite Si- and SiO_2-posts, respectively. (b) The calculated spatial distributions of stationary temperature of the microdisk on various Si posts with sizes of 1.8 (i), 2.4 (ii), and 3.0 μm (iii), respectively. The temperatures in (i)-(iii) were normalized with respect to the maximum value of (i). The scale bar in (i) is 2 μm. The enlarged Si-post facilitated the heat transfer to cool down the microdisk, resulting in the decreased average temperature. (c) The calculated average temperature of the microdisk on a planar SiO_2/Si substrate as a function of the thickness of SiO_2 layer. The red and blue dotted lines indicated the microdisk on Si- and SiO_2-only substrates, respectively. (d) The calculated spatial distributions of stationary temperature of the microdisk on various SiO_2/Si substrates with SiO_2 thicknesses of 0.2 (i), 0.6 (ii),

and 1.0 μm (iii), respectively. The temperatures in (i)-(iii) were normalized with respect to the maximum value of (iii). The scale bar in (i) is 2 μm. Here, the SiO_2 layer was introduced to describe either a thin oxidation layer or a low-index polymer structure in the conventional hybrid integration devices. The increased SiO_2 thickness with low thermal conductivity limited the efficient heat transfer through the Si substrate, which caused the increased temperature in the microdisk.

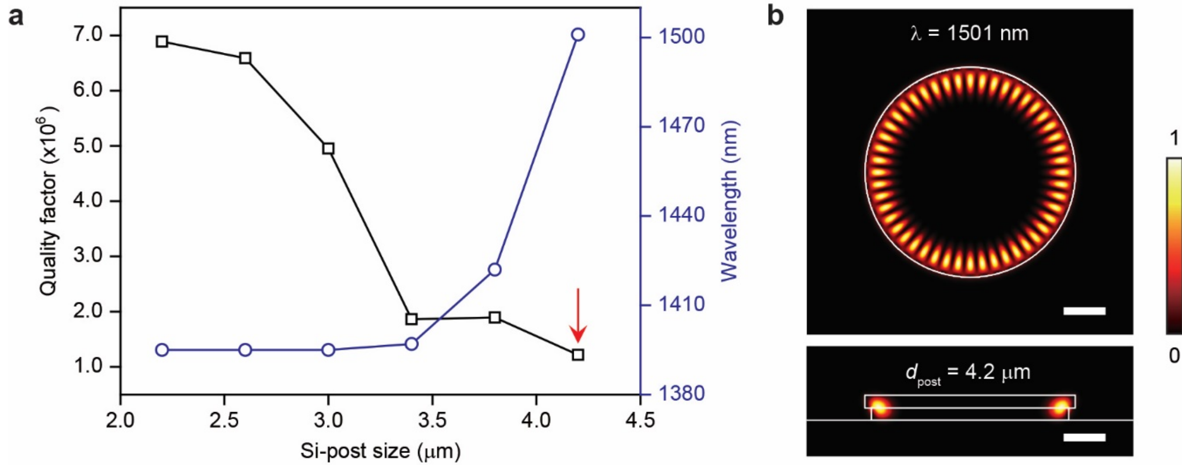

Figure S11. Optical properties of the WGM with an azimuthal order of 24. (a) Calculated *Q*-factor and resonant wavelength as a function of Si-post size. (b) Top and side views of the calculated intensity distributions of WGM excited on the microdisk on Si-post with d_{post} of 4.2 μm.